Polymer Chemistry

PAPER

View Article Online
View Journal | View Issue

Cite this: *Polym. Chem.*, 2018, **9**, 3108

A biocompatible diazosulfonate initiator for direct encapsulation of human stem cells *via* two-photon polymerization†

Maximilian Tromayer,‡[a,e] Agnes Dobos,‡[b,e] Peter Gruber,[b,e] Aliasghar Ajami,[c] Roman Dedic,[d] Aleksandr Ovsianikov[b,e] and Robert Liska*[a,e]

Direct cell encapsulation is a powerful tool for fabrication of biomimetic 3D cell culture models *in vitro*. This method allows more precise recapitulation of the natural environment and physiological functions of cells compared to classical 2D cultures. In contrast to seeding cells on prefabricated scaffolds, cell encapsulation offers benefits regarding high initial cell loading, uniformity of cell distribution and more defined cell–matrix contact. Two-photon polymerization (2PP) based 3D printing enables the precise engineering of cell-containing hydrogel constructs as tissue models. Two-photon initiators (2PIs) specifically developed for this purpose still exhibit considerable cyto- and phototoxicity, impairing the viability of encapsulated cells. This work reports the development of the first cleavable diazosulfonate 2PI DAS, largely overcoming these limitations. The material was characterized by standard spectroscopic methods, white light continuum two-photon absorption cross-section measurements, and its photosensitization of cytotoxic singlet oxygen was compared to the well-established 2PI P2CK. When DAS is used at double concentration to compensate for the lower two-photon cross section, its performance in 2PP-printing of hydrogels is similar to P2CK based on structuring threshold and structure swelling measurements. PrestoBlue metabolic assay showed vastly improved cytocompatibility of DAS in 2D. Cell survival in 3D direct encapsulation *via* 2PP was up to five times higher *versus* P2CK, further demonstrating the excellent biocompatibility of DAS and its potential as superior material for laser-based biofabrication.

Received 15th February 2018,
Accepted 7th May 2018

DOI: 10.1039/c8py00278a

rsc.li/polymers

Introduction

Hydrogels are cross-linked 3D networks of hydrophilic polymers extensively swollen with water.[1] They are an important class of scaffold materials, which are able to mimic roles of the non-cellular component of tissues, the extracellular matrix (ECM), such as providing essential cues for cell adhesion and proliferation, while allowing the diffusion of nutrients, metabolites and growth factors.[2] The polymers employed can be based on either synthetic materials *e.g.* poly(ethylene glycol) or naturally derived materials, such as collagen, fibrin, alginate or hyaluronic acid. Gelation can happen through a variety of mechanisms where polymer chains are cross-linked by covalent, ionic, or physical bonds. While naturally occurring hydrogels are typically cross-linked by physical or ionic mechanisms, covalently cross-linked hydrogels are becoming more attractive due to better stability, tunability of mechanical properties and degradation.[3] Gelatin, derived from collagen, exhibits excellent cell adhesion, biocompatibility and biodegradability.[4–7] Because its natural physical gelation is inhibited at physiological temperatures, methacrylamide functionalities are introduced on gelatin's primary amine groups, enabling covalent cross-linking *via* photopolymerization to facilitate its use as scaffold material.[8]

3D cell encapsulation is a powerful tool for tissue engineering, not only offering the benefits of cellular environments mimicking physiological tissues closer than classical 2D culture models, but also being advantageous to the general approach of seeding cells on porous prefabricated scaffolds.[3,9,10] Compared to the latter method, direct encapsulation within the scaffold is a desirable alternative providing high initial cell loading, uniform cell distribution and more

[a]*Institute of Applied Synthetic Chemistry, TU Wien (Technische Universitaet Wien), Getreidemarkt 9/163/MC, 1060 Vienna, Austria. E-mail: robert.liska@tuwien.ac.at*
[b]*Institute of Materials Science and Technology, TU Wien (Technische Universitaet Wien), Getreidemarkt 9/308, 1060 Vienna, Austria*
[c]*Faculty of Physics, Semnan University, 35131-19111 Semnan, Iran*
[d]*Faculty of Mathematics and Physics, Department of Chemical Physics and Optics, Ke Karlovu 3, Charles University, 12116 Praha 2, Czech Republic*
[e]*Austrian Cluster for Tissue Regeneration, Austria. http://www.tissue-regeneration.at/*
†Electronic supplementary information (ESI) available. See DOI: 10.1039/c8py00278a
‡These authors contributed equally to this work.

intimate cell–matrix contact.[11] Furthermore, the concomitant presence of cells during scaffold fabrication allows for high throughput, streamlining the process towards automated tissue fabrication.[12]

Several additive manufacturing technologies (AMTs) have been used in tissue engineering and regenerative medicine, allowing the automated and reproducible production of complex 3D constructs for cell growth from a variety of materials and in accordance with computer-aided design (CAD) models.[13,14] In 3D bioprinting, cells are suspended in a biocompatible matrix material (usually hydrogel based) to form a bioink, which is deposited in a layer-by-layer manner *via* extrusion, inkjet or laser-assisted strategies, however these methods are often time consuming or result in low resolution structures.[15–18] Stereolithography using photopolymerization induced by UV-lasers has been employed to fabricate 3D hydrogel constructs combining multiple cell and material types patterned in predetermined regions.[12,14] Another powerful 3D printing approach is based on two-photon polymerization (2PP), where nonlinear absorption of a tightly focused, femtosecond laser pulses leads to localized cross-linking of photosensitive materials within the focal volume.[19] Since many photosensitive materials are essentially transparent to the utilized laser wavelength (usually near-infrared), the need for a layer-by-layer deposition process used in other AMTs is avoided and structures can be produced directly within the bulk of the sample. Arbitrary 3D structures with feature sizes ranging from less than 100 nm to 100 μm can be manufactured, closing the existing gap in structural parameters of scaffolds fabricated by different methods.[20–23] Furthermore, 2PP enables selective covalent cross-linking within photosensitive gelatin while used as effectively solid physical gel, thus avoiding gravitational sinking encountered during the encapsulation process in cell suspensions.[21,24] This ensures a homogeneous distribution of cells throughout fabricated 3D constructs.

2PP has been employed using rose bengal as photosensitizer to fabricate micropillars from bovine serum albumine as artificial stem cell niches, as well as cross-linking cytoplasmic proteins inside live starfish oocytes to create barriers and channels isolating different intracellular regions, with the aim of conducting functional studies.[25,26] Direct 3D encapsulation of polymicrobial bacterial communities *via* 2PP has also been achieved.[27] However, there is still a lack of studies demonstrating more sensitive cell types kept viable after successful 2PP encapsulation. This is in part due to the limitations associated with currently available photosensitizers and photoinitiators (PIs) used to start the covalent cross-linking processes, such as free radical polymerization.

Classical UV-encapsulation of cells has made use of commercial PIs such as Irgacure 2959, VA-086 and Li-TPO-L (see Fig. 1), which generate initiating radicals by homolytic bond cleavage upon photoexcitation.[11,28–30] Due to their relatively small conjugated π-systems, classical UV-PIs generally have low two-photon absorption cross sections (σ_{2PA}) and tend to suffer from poor performance and low achievable writing speeds in 2PP.[31,32] Thus, specialized water-soluble two photon initiators (2PIs) such as P2CK (see Fig. 1) have been developed and proved highly efficient in the microfabrication of 3D hydrogel structures.[33] Nonetheless, these 2PI systems exhibit significant cytotoxicity above certain concentrations even in the absence of light, and can cause extensive photodamage to cells after laser irradiation. We reported such photodamage in previous studies and hypothesized that P2CK can photosensitize the formation of cytotoxic reactive oxygen species (ROS) such as singlet oxygen ($^1O_2$).[21] This would be in accordance with sensitized $^1O_2$-formation well described in literature for rose bengal, and in case of P2CK similar to and competing with the hypothetical mechanism of bimolecular generation of 2PP initiating radicals.[26,34,35] Since aforementioned cleavable commercial PIs have shown good cytocompatibility in UV-encapsulation of cells, we hypothesize that generation of polymerization initiating radicals by rapid, unimolecular 2PI cleavage could help minimize unwanted side-processes associated with bimolecular initiation mechanisms of conventional 2PIs during long lived triplet state.

Aryl diazosulfones cleave under formation of phenyl- and sulfonyl-based radicals as well as molecular nitrogen, and have been used for thermally induced free radical polymerization.[36] Their use in 2PP has not been previously reported in literature,

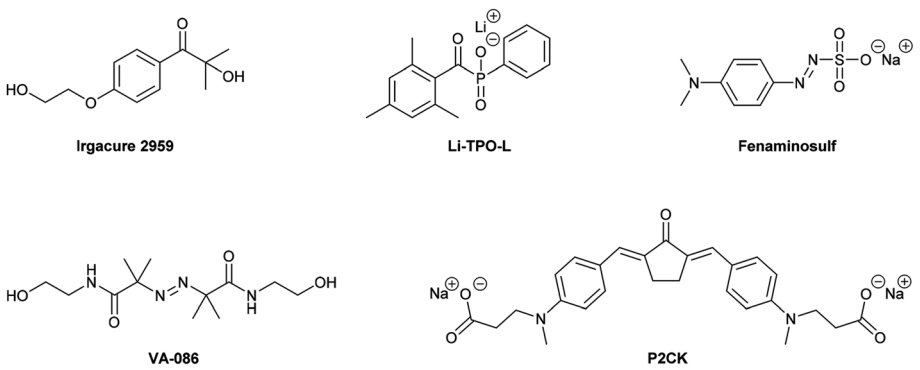

Fig. 1 Chemical structures of the photoinitiators discussed in this publication.

but they exhibit strong absorption in the visible range that was suspected to also be excited by two-photon absorption (2PA) at 800 nm.

The objective of the present study was to develop a water-soluble, cleavable aryl diazosulfonate 2PI with excellent cyto-compatibility, transcending the limitations of state-of-the-art materials. The novel 2PI's properties were characterized and compared to the reference material P2CK by standard spectroscopic methods, white light continuum (WLC) spectral σ_{2PA} measurements, $^1O_2$ luminescence determination as well as experiments examining 2PP structuring threshold and swelling behavior of cross-linked hydrogel structures. 2D and 3D *in vitro* biocompatibility was evaluated by using adipose-derived stem cells (ASC/TERT1) in cell viability assays both in the absence of light and after direct cell encapsulation *via* 2PP.

Experimental

Materials and methods

Chemicals for synthesis. 4,4′-Diaminostilbene-2,2′-disulfonic acid (amsonic acid) was purchased from TCI Europe and used without further purification. Hydrochloric acid, $NaNO_2$, K_2SO_3 and K_2CO_3 were purchased from Sigma-Aldrich and used without further purification. Solvents and other reagents were purchased from Sigma Aldrich, Fluka, Merck and Riedel-de Haen and were either used without further purification or dried and purified by standard laboratory methods. P2CK free acid was prepared according to literature.[33] The sodium salt used in this publication was obtained by dissolving P2CK in aqueous NaOH at 50 °C to a pH of 7.2 and freeze-drying the filtered solution.

Mode of practice for photosensitive compounds. The preparation and analysis of the photosensitive compounds and formulations was conducted in an orange light lab. The windows and fluorescent lamps were covered with foil filters or filter coatings so that light with a wavelength <520 nm was cut off.

Nuclear magnetic resonance (NMR) spectroscopy. ^{1}H-, ^{13}C- and HSQC-NMR spectra were measured with BRUKER Avance 200, BRUKER Avance 400 and BRUKER Ascend 600 FT-NMR-spectrometers. The chemical shift (s = singlet, bs = broad singlet, d = doublet, t = triplet, m = multiplet) is displayed in ppm using the non deuterated solvent as internal standard. Solvents with a grade of deuteration of at least 99.5% were used and purchased from EURISOTOP.

Synthesis of 4,4′-(1,2-ethenediyl)bis[3-sulfobenzenediazonium]dichloride (TAZ). Hydrochloric acid (6.0 mL, 37% aq.) is added dropwise to a magnetically stirred suspension of amsonic acid (10.0 g, 27.0 mmol, 1.0 eq.) in deionized H_2O (54 mL). The stirred suspension is then cooled in an ice/water bath and a solution of $NaNO_2$ (4.23 g, 61.3 mmol, 2.27 eq.) in H_2O (9 mL) is added dropwise, keeping the temperature below 5 °C. After the addition of $NaNO_2$ is completed, the reaction mixture is stirred at room temperature for 30 min and then at 35 °C for another 2.5 h. The suspension is then cooled to 4 °C, the solids collected by centrifugation (3000 rpm, 10 min) and washed subsequently with deionized H_2O (2 × 40 mL), MeOH (2 × 40 mL) and Et_2O (2 × 40 mL), always collecting the solids *via* centrifugation and discarding the liquid phases. The resulting bright yellow paste TAZ is then carefully dried *in vacuo* at room temperature. Yield: 10.4 g (83% of theory). Mp: decomposition >90 °C; ^{1}H NMR (200 MHz, DMSO-d_6, δ): 9.10 (2H, d, J = 2.2 Hz, Ar–H^2), 8.70 (2H, dd, J = 2.2 and 8.7 Hz, Ar–H^6), 8.52 (2H, s, –CH=CH–), 8.14 (2H, d, J = 8.7 Hz, Ar–H^5).

Synthesis of tetrapotassium 4,4′-(1,2-ethenediyl)bis[2-(3-sulfophenyl)diazenesulfonate] (DAS). Powdered K_2CO_3 (1.48 g, 10.7 mmol, 1.0 eq.) and K_2SO_3 (90% purity, 3.78 g, 21.5 mmol, 2.0 eq.) are mixed homogeneously by shaking and the mixture of solids is added portion-wise to a magnetically stirred suspension of TAZ (5.0 g, 10.7 mmol, 1.0 eq.) in deionized H_2O (35 mL). During the addition of solids the suspension first turns milky-orange and changes to a very dark but clear solution shortly before addition is completed. This solution is first stirred for 18 h at room temperature and then left to crystallize for another 18 h at 4 °C. The precipitate is collected *via* centrifugation, recrystallized by dissolving in the minimal amount deionized water at 70 °C then cooling to 4 °C, and dried *in vacuo* over P_2O_5 to obtain a finely crystalline orange powder. Yield: 3.77 g (50% of theory). Mp: decomposition >300 °C; ^{1}H NMR (600 MHz, D_2O, δ): 8.38 (2H, d, J = 2.2 Hz, Ar–H^2), 8.12 (2H, s, –CH=CH–), 8.11 (2H, d, J = 8.4 Hz, Ar–H^5), 8.06 (2H, dd, J = 2.2 and 8.4 Hz, Ar–H^6); ^{13}C NMR (100 MHz, D_2O, δ): 148.8 (Ar–C^3), 142.0 (Ar–C^4), 139.9 (Ar–C^1), 130.3 (–CH=CH–), 129.4 (Ar–C^5), 126.3 (Ar–C^6), 123.3 (Ar–C^2); anal. calcd for $C_{14}H_8K_4N_4O_{12}S_4$: C 23.72, H 1.14, K 22.06, N 7.90, O 27.08, S 18.09; found: C 23.35, H 1.37, K 22.40, N 7.01, O 28.18, S 17.18.

Spectral properties

UV/Vis-absorption spectra were recorded on a Shimadzu UV/VIS 1800 spectrometer. 2PA spectra were determined using white light continuum (WLC) *Z*-scan.[37] A Ti:sapphire laser system (FEMTOSOURCE COMPACT PRO, Femtolasers GmbH) producing 500 μJ, 30 fs, 800 nm pulses at 1 kHz repetition rate was used as source for WLC generation. The Ti:sapphire laser output beam is slightly focused using a 150 cm focal length plano-convex lens to a 200 μm diameter spot at the entrance of the 250 μm diameter 175 cm long hollow fiber (KALEIDOSCOPE™ hollow fiber compressor) placed inside a chamber filled with argon gas at a pressure of 0.6 bar. This leads to a WLC beam spectrally broadened in the range of 550–1000 nm, which is first transmitted through a set of half-wave plate and polarizer in order to regulate the intensity and subsequently through an ultra-broadband dispersive mirror compressor consisting of 8 mirrors to produce sub-10 fs pulses.

The WLC beam emerging from the compressor was dispersed using an F2-glass prism-pair and then focused into the sample using a 150 mm focal length cylindrical lens. The sample was mounted on a translation stage moving step-wise in the laser beam propagation direction to facilitate *Z*-scans. The nonlinear transmittance was measured by a charge-

coupled-device (CCD) line camera [CCDS3600-D from ALPHALAS (3648 pixels with pixel-width of 8 μm)] as a function of the sample position. Since different spectral components are spatially separated, any part of the sample in the beam cross section is irradiated with almost single wavelength pulses leading to only degenerate 2PA processes. The 2PA cross section at each wavelength can be extracted by fitting eqn (1) to the measured data and thus wavelength resolved degenerate 2PA spectra can be obtained by performing a single *Z*-scan using dispersive WLC.

$$T(z) = \sum_{n=0}^{\infty} \frac{\left(-(\sigma_2 \lambda N_A \rho \times 10^{-3}/hc) L I_0\right)^n}{(n+1)^{3/2}\left(1+\frac{z^2}{z_R{}^2}\right)} \quad (1)$$

where, T is the normalized transmittance, L is the sample thickness, z_R is the Rayleigh range, z is the sample position measured with respect to the focal plane, I_0 is the peak on-axis intensity at the focal plane, h is the Plank constant, c is the light speed in free space, N_A is the Avogadro constant, ρ is the concentration of the examined solution in mol L^{-1}, λ is the wavelength and σ_2 is the 2PA cross section.

Singlet oxygen measurements

The sensitized production of $^1O_2$ by the materials was studied by direct detection of near-infrared luminescence of $^1O_2$ around 1270 nm using a home-built set-up.[38] The sample was irradiated by 5 ns long pulses at 420 nm with ~5 μJ in pulse provided by dye laser (FL1000, Lambda Physik) pumped by excimer laser (ATLEX 500i, ATL Lasertechnik). The luminescence signal was collected through two RG7 long-pass filters (Schott) and high-luminosity monochromator (H20IR, Jobin–Yvon) to the infrared sensitive photomultiplier (R5509, Hamamatsu) working in single photon counting mode. The photomultiplier output was detected by time-resolved multichannel photon counter (MSA-200, Becker-Hickl) with 5 ns per channel resolution. Increase of the signal after increasing the partial oxygen pressure as well as total quenching of the signal by specific $^1O_2$ quencher NaN_3 was used to verify that the obtained luminescence kinetics originates only in $^1O_2$. The kinetics obtained with the quencher was subtracted as a background before analysis of the $^1O_2$ kinetics. 300 000 sweeps were accumulated to obtain each kinetics. The lifetimes of $^1O_2$ were obtained by fitting a model based on single-exponential decays of both the sensitizer and the $^1O_2$.

ASC/TERT1 cell culture

ASC/TERT1 (Evercyte, Vienna, Austria) were cultured and maintained in EGM-2 media (Lonza, Basel, Switzerland) supplemented with fetal bovine serum (FBS) (Sigma-Aldrich, Saint Louis, MO, USA) to a final concentration of 10%. Cells were incubated in a humidified atmosphere with 5% CO_2 at 37 °C. At 80% confluence the cells were detached using 0.5% trypsin–EDTA solution (Gibco, Waltham, MA, USA) and after the cells detached trypsin inhibitor was added (Gibco, Waltham, MA, USA), the cells were resuspended in media and centrifuged at 170*g* for 5 min before seeding onto T75 flasks.

Cell viability

Cell viability was measured using PrestoBlue Assay (Invitrogen, Carlsbad, CA, USA). Briefly, cells were seeded in 96-well culture plates. 0.5–4 mM DAS and P2CK solution in EGM-2 (10% FBS) media was added to the wells (followed by a 10 min UV irradiation on one plate) and the plates were incubated for 3 h at 37 °C. Afterwards the cells were washed with PBS (Sigma-Aldrich, Saint Louis, MO, USA) twice before fresh media was added and the cells were left to recover overnight. After 24 h PrestoBlue assay was performed, by diluting the reagent 1 : 10 with EGM-2 media and the plates were incubated for 1 h. The absorbance was measured in a plate reader at an excitation wavelength of 560 nm and the emission was recorded at 590 nm. Data were analyzed with GraphPad Prism software using one-way ANOVA with Kruskal–Wallis test followed by Dunn's multiple comparisons *post-hoc*.

DNA quantification

FlouReporter Blue Fluorometric dsDNA Quantitation Kit (Thermo-Fisher, Waltham, MA, USA) was used to measure the DNA content of the samples after treatment with the photoinitiators. The plates on which PrestoBlue assay was applied were frozen for 5 days at −80 °C and Hoechst assay was preformed following the instructions of the manufacturer. Briefly, the plates were thawed at room temperature and 100 μL distilled water was added and the plates were incubated at 37 °C for 1 h. Afterwards, Hoechst 33258 staining was diluted to 1 : 400 with TNA buffer (10 mM Tris, 2 M NaCl, 1 mM EDTA, 2 mM sodium azide), 100 μL of the reagent was added to the wells and the fluorescence was measured using excitation and emission filters at 369 nm and 460 nm, respectively.

2PP setup

For 2PP structuring, a femtosecond NIR-laser (MaiTai eHP DeepSee, Spectra-Physics) was used at 800 nm, with a repetition rate of 80 MHz and a pulse duration of 70 fs after the microscope objective (Plan-Apochromat 10×/0.3, Zeiss). The peak intensity for these parameters at 1 mW average power is 7 GW cm^{-2} in the focal plane of the objective and the spectral width of the used laser system at 800 nm is 9.6 nm; the detailed calculation of these values is described elsewhere.[39] To facilitate high-speed structuring a combination of sample positioning *via* a motorized stage and a galvo-scanner was used for laser beam positioning within the sample. The in-house developed software controls the complete setup. The structuring process was monitored in real time with a CMOS-camera mounted behind the dichroic mirror in the beam path.

Methacrylation of glass surfaces

Methacrylation of glass bottom dishes (35 mm diameter with glass bottom, high version, Ibidi GmbH, Martinsried, Germany) was performed according to literature.[39]

Structuring threshold

In order to evaluate the structuring threshold of the hydrogels, 10% gelatin methacrylamide hydrogel (GelMOD) with a substitution rate of 95%, (provided by Ghent University) was dissolved in EGM-2 media supplemented with 1 mM P2CK or 2 mM DAS. Cubes with a side length of 100 μm were printed on methacrylated glass using the previously mentioned 2PP setup, with different writing speeds (100–1000 mm s^{-1}), different powers (45–100 mW), and hatching with 0.5 μm line and 0.5 μm layer spacing. The threshold was defined as the minimal power needed for structuring.

Swelling

The swelling ratio of samples (10% GelMOD with 1 mM P2CK or 2 mM DAS) was addressed by measuring the changes in perimeter of the samples using ImageJ FIJI software. 100 μm cubes were printed using parameters above the structuring threshold. The printed structures were immersed in PBS for 48 h until they reached the swelling equilibrium. The swelling ratio (Q) was calculated using eqn (2):

$$Q = \frac{\mathrm{Pt} - \mathrm{Pb}}{\mathrm{Pb}} \times 100 \quad (2)$$

where, Pt is the perimeter of the cubes on the top, Pb is the perimeter of the sample on the bottom.

Cell encapsulation

ASC/TERT1 cells were trypsinized, and resuspended in 10% GelMOD solution supplemented with either 1 mM P2CK or 2 mM DAS at a concentration of 2×10^6 cells per mL. The cell-containing hydrogel precursor solution was applied to methacrylated μ-dishes (35 mm diameter with glass bottom, high version, Ibidi GmbH, Martinsried, Germany). The structures were printed with the above mentioned 2PP setup, using 0.5 μm line and 0.5 μm layer spacing. In order to assess the changes in cell numbers, larger cubes of 300 μm cubes were printed, using 1000 mm s^{-1} writing speed. For demonstration TU logos were printed with a writing speed of 250 mm s^{-1}. The viability of cells was assessed with calcein AM/propidium iodide staining (Sigma-Aldrich, St Luis, USA). The samples were incubated for 20 min before the images were captured by confocal laser scanning microscope (LSM700 Zeiss, Germany).

Results and discussion

Synthesis

Diazosulfones and the closely related, water-soluble diazosulfonates have been employed for a wide array of uses, ranging from building blocks and reagents in organic synthesis to radical polymerization, film coatings, diazo copying and fungicides.[36,40,41] After preliminary 2PP experiments showed that commercially available sodium [4-(dimethylamino)phenyl]diazenesulfonate (fenaminosulf, see Fig. 1) is a relatively efficient 2PI considering that its conjugated π-system is small, which is usually associated with low σ_{2PA}, a series of diazosulfonates with extended π-systems was prepared, most of them practically insoluble in water. Therefore two strongly hydrophilic sulfonate moieties were attached on the aromatic core of the 2PI to achieve the excellent water solubility of the novel 2PI presented in this study, tetrapotassium 4,4′-(1,2-ethenediyl)bis [2-(3-sulfophenyl)diazenesulfonate] (DAS).

In the first step of the synthetic sequence to obtain DAS (see Fig. 2), amsonic acid was converted to its tetrazonium salt (TAZ) *via* a diazotization procedure adapted from literature.[42] Diazosulfonates are typically prepared by coupling the corresponding diazonium salts with alkali sulfite (usually Na_2SO_3) in aqueous solution, leading to precipitation of the product. However, in case of DAS the solubility of the sodium salt is so high that it does not readily precipitate from the reaction mixture. Thus a mixture of K_2CO_3 to neutralize the sulfonic acid groups of TAZ and K_2SO_3 as sulfite source was used to successfully isolate DAS, in accordance with literature suggesting a generally lower solubility of potassium diazosulfonates compared to the sodium salts.[43]

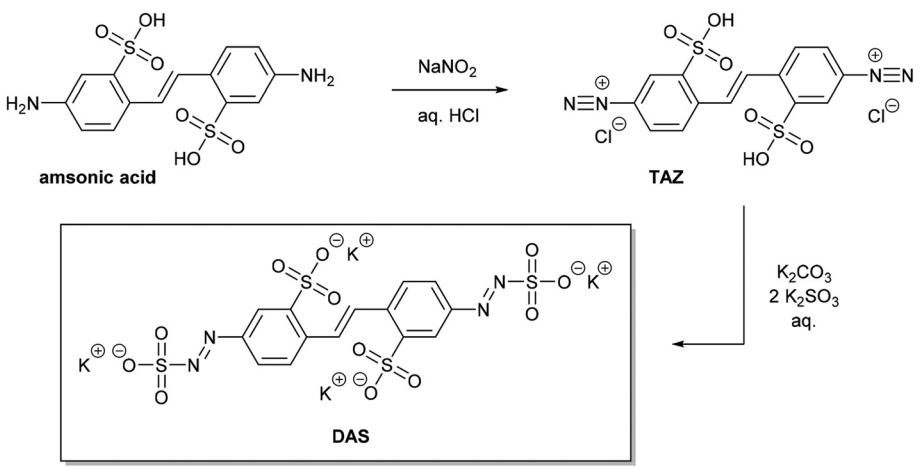

Fig. 2 Scheme of the synthetic pathway to DAS.

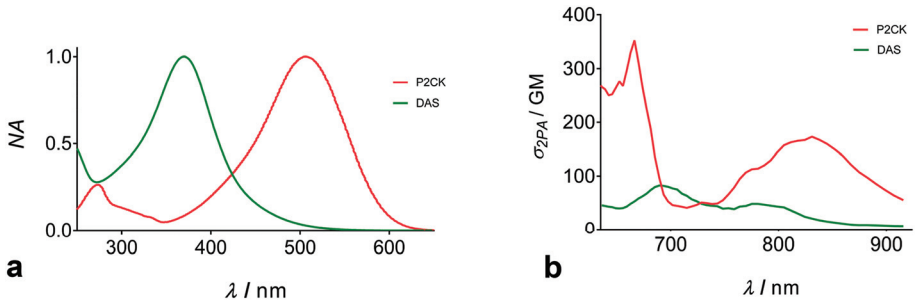

Fig. 3 (a) UV/VIS normalized absorption spectra. The absorption maximum of DAS is blue-shifted (λ_{max} = 370 nm) and the specific absorption lowered ($\varepsilon_{\lambda_{max}}$ = 22 000 L mol^{-1} cm^{-1}) compared to P2CK (λ_{max} = 506 nm, $\varepsilon_{\lambda_{max}}$ = 55 000 L mol^{-1} cm^{-1}) (b) WLC 2PA spectra of DAS and the reference P2CK. The σ_{2PA} of DAS is around 40 GM at the 2PP structuring wavelength used (800 nm), while P2CK has a more than three times higher σ_{2PA} of about 140 GM at this wavelength.

Spectral properties

In UV/Vis-spectra (Fig. 3a) DAS shows a more blue-shifted absorption maximum (λ_{max} = 370 nm) as well as a lower specific absorption ($\varepsilon_{\lambda_{max}}$ = 22 000 L mol^{-1} cm^{-1}) in comparison to P2CK (λ_{max} = 506 nm, $\varepsilon_{\lambda_{max}}$ = 55 000 L mol^{-1} cm^{-1}). Both result from DAS bearing sulfonate and diazosulfonate groups acting as electronic acceptors, while P2CK has strong dialkylamino electronic donor groups causing intensification and red-shift of the linear absorption.

Similar effects are observed in case of the white light continuum (WLC) 2PA spectra (Fig. 3b). The 2PA cross section of DAS is around 40 GM at the 2PP structuring wavelength used (800 nm), while P2CK has a more than three times higher cross section of about 140 GM. However, the resulting lower 2PP structuring efficiency of DAS can be sufficiently compensated by using a concentration of 2 mM, *versus* 1 mM for P2CK, to obtain good 2PP processing results.

Singlet oxygen measurements

Oxidative damage to cells and tissues caused by $^1O_2$, generated with the aid of a photosensitizer, has been exploited in photodynamic therapy (PDT) for medical purposes.[44] However, during 2PP encapsulation of cells such phototoxicity should ideally be completely avoided. The direct time-resolved detection of $^1O_2$ infrared luminescence at 1270 nm was employed to determine the formation of $^1O_2$ sensitized by P2CK and DAS respectively. 2PI solutions were irradiated at 420 nm. At 1 mM, a concentration typically used for 2PP structuring, P2CK showed only a very weak signal in the first 1 μs after the excitation pulse. The lifetime of $^1O_2$ in water is naturally short (3.5 μs), so D_2O (~68 μs lifetime) was used as a solvent for further measurements to obtain better signal quality due to higher quantum yield of phosphorescence.[45,46] The signal was also improved by lowering P2CK concentration to 0.1 mM. Further lowering P2CK concentration to 20 μM led to almost disappearing luminescence signal. This indicates that P2CK acts both as sensitizer and quencher in the formation of $^1O_2$, with the quenching effect being dominant at 1 mM. The quenching of $^1O_2$ by P2CK is also documented in the shortening of $^1O_2$ lifetime to (16 ± 4) μs (uncertainty obtained as asymptotic standard error during non-linear least-squares fitting) with respect to pure D_2O (Fig. 4, red line).

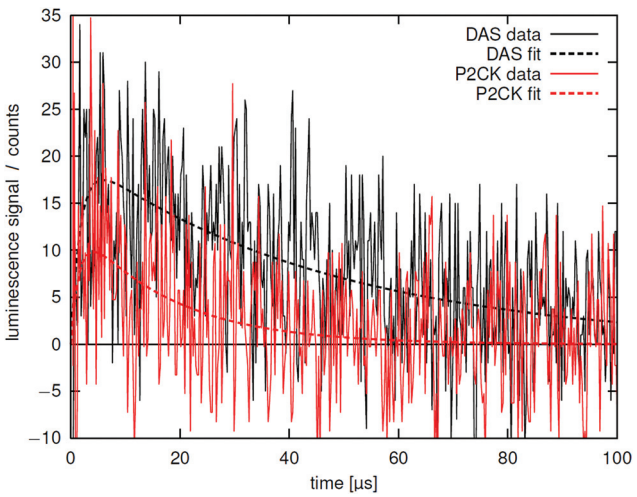

Fig. 4 Luminescence signal (solid) of excited $^1O_2$ generated by 100 μM DAS (black) and the reference P2CK (red) in D_2O saturated by oxygen together with respective fits (dotted).

Contrary to what was expected, DAS (Fig. 4, black line) exhibited a four times stronger signal than P2CK, indicating that it acts as a more potent photosensitizer of $^1O_2$. This can be explained by the fact that the quenching of $^1O_2$ by DAS is much lower compared to P2CK. This conclusion is also supported by the longer $^1O_2$ lifetime of ~40 μs using DAS in D_2O. Nevertheless, the efficiency of $^1O_2$ generation is exceedingly weak in both cases. It is two to three orders of magnitude lower compared to compounds used in PDT such as porphyrins (compared to tetraphenylporphine tetrasulfonate (TPPS4) in the same experimental setup, data not shown).[47,48] Therefore we hypothesize that $^1O_2$-formation alone is not the only cause of photodamage observed in the 2PP-encapsulation of cells with P2CK.

2D cell viability

PrestoBlue mitochondrial activity assay was used to address the viability of adipose derived stem cells (ASC/TERT1) in 2D.

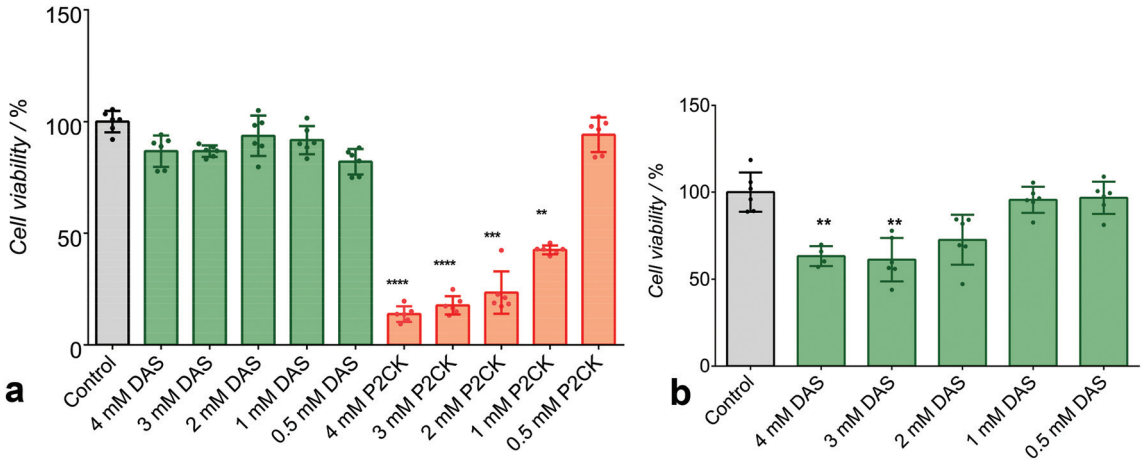

Fig. 5 Quantification of cell viability and number of ASC/TERT1 cells 24 h after treatment with 2PIs DAS and P2CK. Presto blue assay was used evaluate the metabolic activity of the cells. (a) DAS was well tolerated in the analyzed range (0.5–4 mM), while all concentrations of P2CK above 0.5 mM affected cell viability significantly. (b) When the cells were irradiated with UV to model the initiation of the 2PIs, cell viability was maintained up to 2 mM DAS concentration. The statistical significance was addressed by ANOVA with Kruskal–Wallis test followed by Dunn's multiple comparisons test. $n = 6$; $^{**}p < 0.01$; $^{***}p < 0.001$; $^{****}p < 0.0001$.

PrestoBlue reagent is a resazurin-based, cell-permeant solution that uses the reducing power of mitochondrial enzymes of living cells to quantitatively measure proliferation.[49] 24 h after stimulation with different concentrations of 2PIs the cells exhibited normal metabolic activity in case of DAS, while P2CK treatment led to significant decrease of cell viability above 0.5 mM (Fig. 5a).

These results were in accordance with DNA quantification using Hoechst 33258 staining, a dye that stains double stranded DNA, and therefore corresponds to the actual cell number of the sample (Fig. S4†).[50] The drawback of this method is that partial precipitation of P2CK in the samples interferes with the measurement of fluorescence intensity at the required wavelengths leading to unreliable results. Therefore, this method of DNA quantification could only be used for the DAS samples. In a further experiment, a plate containing 2PIs was irradiated at 365 nm in order to mimic the photoinitiation process. This additional step resulted in significantly lower survival of stem cells above 2 mM DAS concentration, however even at 3 mM and 4 mM the cell survival reached 60% compared to the untreated control (Fig. 5b). The DNA quantification also corresponded with the experienced results shown in Fig. S4B.† On the other hand, these conditions led to apoptosis in all samples treated with any concentrations of P2CK (not plotted).

Structuring threshold

DAS was tested in 2PP processing and compared to the well-established 2PI P2CK. In order to investigate the laser power threshold for structuring, a 10% GelMOD hydrogel supplemented with 1 mM P2CK or 2 mM DAS was prepared and 100 μm cubes were printed at 45–100 mW and up to 1 m s^{-1} writing speed. The applied 2PI concentrations were kept as low as possible, while still reaching fabrication threshold at an acceptable laser power. Fig. 6a shows that although 1 mM P2CK needs an average 15 mW less power at every given

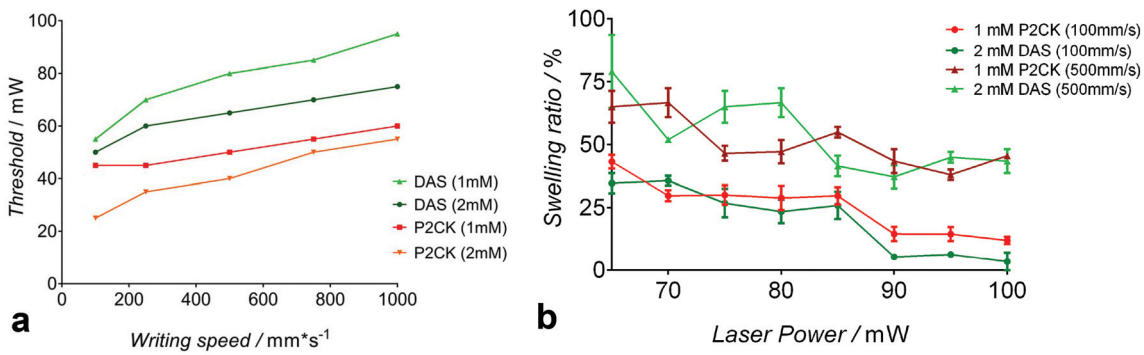

Fig. 6 2PP processing of hydrogels. (a) Structuring threshold of 2PIs. At all tested writing speeds it was possible to structure in the gels using either 2PI. P2CK (red) required less laser power in comparison to DAS (green). (b) Swelling of hydrogels fabricated at different writing speeds of 100 mm s^{-1} and 500 mm s^{-1}. The swelling was power and speed dependent and comparable in both cases.

writing speed to reach the threshold limit, it is possible to use 2 mM DAS as a suitable alternative to P2CK for 2PP application.

Swelling properties of 2PP fabricated hydrogels

The swelling profile of a hydrogel demonstrates its ability to absorb water, which is related to the cross-linking density of the material, hence the stiffer the gel is, the less it swells. It affects not only the diffusion rate of nutrients and metabolites in the hydrogel, but also the migration and stretching of cells. Besides the 2PI and hydrogel polymer concentrations, the laser power and writing speed affect the number of cross-links within the gel. In order to study the swelling of the samples, a set of 100 μm cubes were fabricated with different writing speeds and powers, using 10% GelMOD supplemented with either 1 mM P2CK or 2 mM DAS. After the samples reached equilibrium state (approximately after 48 h) the swelling was recorded.

Both the writing speed and the laser power influenced the swelling behavior of the hydrogels as expected (Fig. 6b). Increased speed and decreased power led to more extensive swelling regardless of the 2PI used, and both 2PIs led to similar results under these circumstances. For this reason 2 mM of DAS can be used as a substitute for 1 mM P2CK to reach the similar cross-linking density of material.

Encapsulation of ASC/TERT1 cells using 2PP

In order to evaluate the biocompatibility of the 2PIs in 2PP processing, ASC/TERT1 cells were encapsulated in 10% GelMOD-95 hydrogel using 1 mM P2CK or 2 mM DAS and followed through the course of 5 days. To facilitate high through-

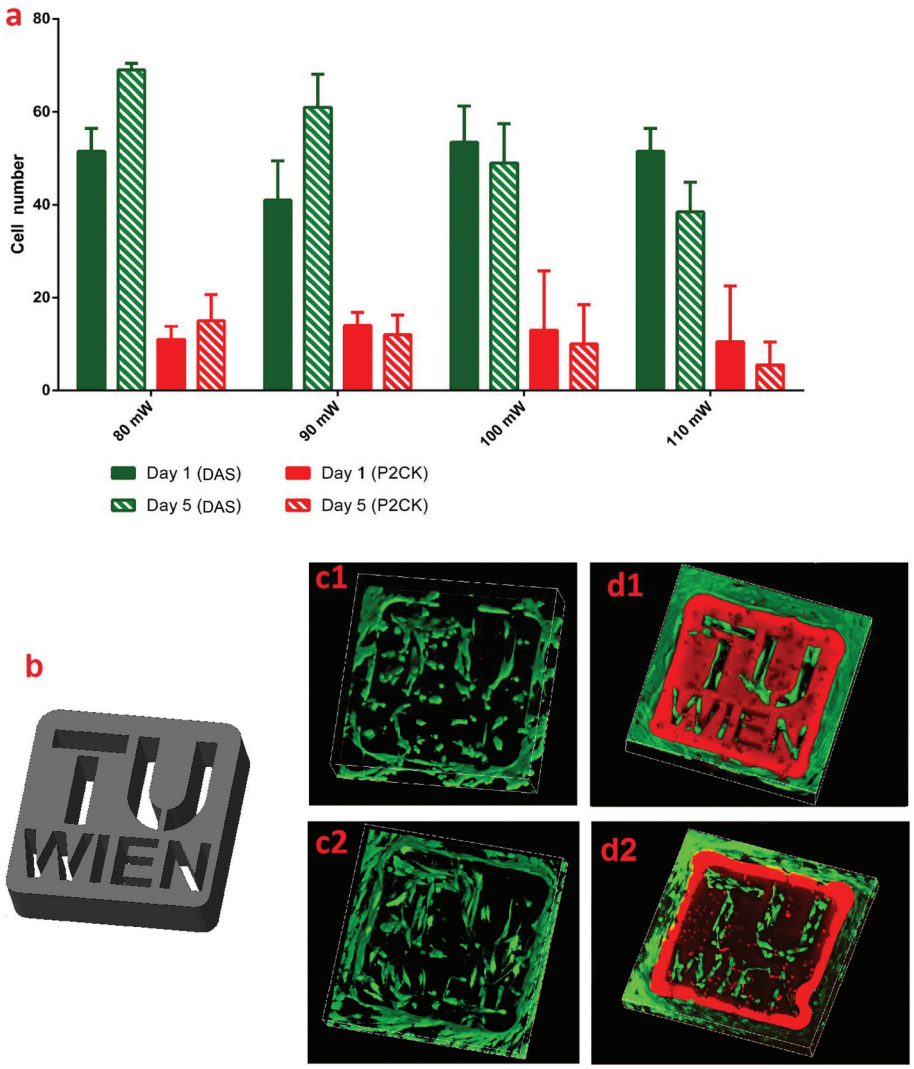

Fig. 7 Survival and proliferation of ASC/TERT1 cells in 2PP-produced GelMOD hydrogel constructs. (a) Number of cells within the 3D printed hydrogel cubes at day 1 and day 5. The application of DAS as 2PI resulted in higher initial higher cell survival and increased proliferation when compared to P2CK. (b) CAD image of printed TU Wien logos, dimensions 500 × 500 × 125 μm (c1) TU Wien logo produced at 80 mW using 2 mM DAS 24 h after 2PP structuring (c2) TU Wien logo structured with 2 mM DAS after 5 days, with high survival and expanded morphology of the cells (d1) TU Wien logo structured with 1 mM P2CK 24 h after fabrication (d2) TU Wien logo structured with 1 mM P2CK after 5 days. Cells were only growing in the void, while cells in the gel were not viable after 5 days.

put, relatively high powers (80–110 mW) were chosen to allow a writing speed as fast as 1 m s^{-1}. The cells were automatically counted using ImageJ FIJI software with an automatic object counting. Although the same amount of cells were encapsulated in both cases, P2CK samples resulted in average 75% less cell survival on day 1, and led to more decrease over the course of time at laser powers above 80 mW. By using DAS, the proliferation of the cells reached up to 140% after 5 days when laser powers below 100 mW were used. However, at higher powers cell numbers decreased, possibly due to too tightly cross-linked hydrogels which did not support proliferation of ASC/TER1 cells. The survival of the cells was dose dependent and reached up to 140% when laser powers under 100 mW were used (Fig. 7a).

To further demonstrate the capacities of DAS as a cytocompatible 2PI, ASC/TERT1 cells were encapsulated in a structure containing not only cross-linked, but also non-polymerized sections (Fig. 7b), and were stained on day 1 and day 5, using calcein AM/propidium iodide live/dead staining. In the P2CK samples, the auto-fluorescence of the 2PI makes the visualization of dead cells challenging, however the cells were only proliferating in the void areas (Fig. 7d). On the other hand in DAS samples no auto-fluorescence was detected, the encapsulated cells were expanding in the gel as well and still responded to the live stain after 5 days (Fig. 7c).

Conclusions

A novel water-soluble diazosulfonate two-photon initiator DAS was prepared from inexpensive commercial starting materials *via* a tetrazonium salt intermediate and compared to the well-established initiator P2CK as a reference. Due to its lower two-photon absorption cross-section, DAS had to be used at double the concentration of P2CK in two-photon polymerization (2PP) structuring. At this concentration DAS supports exceedingly high writing speeds up to 1 m s^{-1} and a performance generally similar to P2CK, as indicated by laser power threshold and hydrogel swelling experiments. It was hypothesized that due to a fast unimolecular cleavage to generate initiating radicals, DAS would photosensitize the formation of undesired, cytotoxic singlet oxygen less efficiently than P2CK. Singlet oxygen luminescence experiments demonstrated that DAS was in fact a better sensitizer than P2CK, however only traces were generated in both cases, indicating that photodamage of cells during 2PP is likely caused by a different mechanism. 2D cell viability assays and 3D cell encapsulation *via* 2PP using adipose derived stem cells both demonstrated the biocompatibility of DAS far exceeding the reference P2CK and its potential as superior material for cell-based biofabrication.

Conflicts of interest

There are no conflicts to declare.

Acknowledgements

The authors thank Prof. Dr Sandra Van Vlierberghe and Prof. Dr Peter Dubruel (Polymer Chemistry and Biomaterials Group, Ghent University, Belgium) for providing methacrylated gelatin (GelMOD). Elemental analysis was carried out by J. Theiner (University of Vienna, Microanalytical Laboratory). Financial support by European Research Council (Starting Grant – 307701, A. O.), the Austrian Science Fund (FWF): P 27555 and the TU Wien doctorate school Biointerfaces is gratefully acknowledged.

References

1 E. M. Ahmed, *J. Adv. Res.*, 2015, **6**, 105–121.
2 M. M. Rahman, E. D. Giol, G. Cama, S. Van Vlierberghe and P. Dubruel, in *Smart Materials for Tissue Engineering*, Royal Society of Chemistry, Cambridge, 2017, pp. 62–99.
3 G. D. Nicodemus and S. J. Bryant, *Tissue Eng., Part B*, 2008, **14**, 149–165.
4 R. P. Scherer Corporation, *US* 4780316A, 1986.
5 W.-M. Hsu, K.-H. Chen, J.-Y. Lai and G.-H. Hsiue, *J. Exp. Clin. Med.*, 2013, **5**, 56–64.
6 S. Sakai, K. Hirose, K. Taguchi, Y. Ogushi and K. Kawakami, *Biomaterials*, 2009, **30**, 3371–3377.
7 M. Nikkhah, M. Akbari, A. Paul, A. Memic, A. Dolatshahi-Pirouz and A. Khademhosseini, in *Biomaterials from Nature for Advanced Devices and Therapies*, John Wiley & Sons, Inc., Hoboken, New Jersey, 2016, pp. 37–62.
8 J. Van Hoorick, P. Gruber, M. Markovic, M. Tromayer, J. Van Erps, H. Thienpont, R. Liska, A. Ovsianikov, P. Dubruel and S. Van Vlierberghe, *Biomacromolecules*, 2017, **18**, 3260–3272.
9 E. Cukierman, R. Pankov, D. R. Stevens and K. M. Yamada, *Science*, 2001, **294**, 1708–1712.
10 M. Bokhari, R. J. Carnachan, N. R. Cameron and S. A. Przyborski, *J. Anat.*, 2007, **211**, 567–576.
11 M. Markovic, J. Van Hoorick, K. Hölzl, M. Tromayer, P. Gruber, S. Nürnberger, P. Dubruel, S. Van Vlierberghe, R. Liska and A. Ovsianikov, *J. Nanotechnol. Eng. Med.*, 2015, **6**, 021001.
12 P. Zorlutuna, J. H. Jeong, H. Kong and R. Bashir, *Adv. Funct. Mater.*, 2011, **21**, 3642–3651.
13 *3D Printing and Biofabrication*, ed. A. Ovsianikov, J. Yoo and V. Mironov, Springer International Publishing, Cham, 2018.
14 X.-H. Qin, A. Ovsianikov, J. Stampfl and R. Liska, *BioNanoMaterials*, 2014, **15**, 49–70.
15 E. Axpe and M. Oyen, *Int. J. Mol. Sci.*, 2016, **17**, 1976.
16 K. Hölzl, S. Lin, L. Tytgat, S. Van Vlierberghe, L. Gu and A. Ovsianikov, *Biofabrication*, 2016, **8**, 32002.
17 M. E. Prendergast, R. D. Solorzano and D. Cabrera, *J. 3D Print. Med.*, 2016, **1**, DOI: 10.2217/3dp-2016-0002.
18 T. Billiet, M. Vandenhaute, J. Schelfhout, S. Van Vlierberghe and P. Dubruel, *Biomaterials*, 2012, **33**, 6020–6041.

19 A. Ovsianikov, V. Mironov, J. Stampfl and R. Liska, *Expert Rev. Med. Devices*, 2012, **4440**, 1–21.
20 A. Ovsianikov, M. Gruene, M. Pflaum, L. Koch, F. Maiorana, M. Wilhelmi, A. Haverich and B. Chichkov, *Biofabrication*, 2010, **2**, 14104.
21 A. Ovsianikov, S. Mühleder, J. Torgersen, Z. Li, X. H. Qin, S. Van Vlierberghe, P. Dubruel, W. Holnthoner, H. Redl, R. Liska and J. Stampfl, *Langmuir*, 2014, **30**, 3787–3794.
22 A. Ovsianikov, A. Gaidukeviciute, B. N. Chichkov, M. Oubaha, B. D. MacCraith, I. Sakellari, A. Giakoumaki, D. Gray, M. Vamvakaki, M. Farsari and C. Fotakis, *Laser Chem.*, 2008, **42**, 1–7.
23 P. E. Petrochenko, J. Torgersen, P. Gruber, L. A. Hicks, J. Zheng, G. Kumar, R. J. Narayan, P. L. Goering, R. Liska, J. Stampfl and A. Ovsianikov, *Adv. Healthcare Mater.*, 2015, **4**, 739–747.
24 M. Tromayer, P. Gruber, M. Markovic, A. Rosspeintner, E. Vauthey, H. Redl, A. Ovsianikov and R. Liska, *Polym. Chem.*, 2017, **8**, 451–460.
25 M. H. Tong, N. Huang, W. Zhang, Z. L. Zhou, A. H. W. Ngan, Y. Du and B. P. Chan, *Sci. Rep.*, 2016, **6**, 20063.
26 S. Basu, V. Rodionov, M. Terasaki and P. J. Campagnola, *Opt. Lett.*, 2005, **30**, 159–161.
27 J. L. Connell, E. T. Ritschdorff, M. Whiteley and J. B. Shear, *Proc. Natl. Acad. Sci. U. S. A.*, 2013, **110**, 18380–18385.
28 N. E. Fedorovich, M. H. Oudshoorn, D. van Geemen, W. E. Hennink, J. Alblas and W. J. A. Dhert, *Biomaterials*, 2009, **30**, 344–353.
29 P. Occhetta, R. Visone, L. Russo, L. Cipolla, M. Moretti and M. Rasponi, *J. Biomed. Mater. Res., Part A*, 2015, **103**, 2109–2117.
30 B. D. Fairbanks, M. P. Schwartz, C. N. Bowman and K. S. Anseth, *Biomaterials*, 2009, **30**, 6702–6707.
31 K. J. Schafer, J. M. Hales, M. Balu, K. D. Belfield, E. W. Van Stryland and D. J. Hagan, *J. Photochem. Photobiol., A*, 2004, **162**, 497–502.
32 M. Pawlicki, H. A. Collins, R. G. Denning and H. L. Anderson, *Angew. Chem., Int. Ed.*, 2009, **48**, 3244–3266.
33 Z. Li, J. Torgersen, A. Ajami, S. Mühleder, X. Qin, W. Husinsky, W. Holnthoner, A. Ovsianikov, J. Stampfl and R. Liska, *RSC Adv.*, 2013, **3**, 15939.
34 P. Klán and J. Wirz, in *Photochemistry of Organic Compounds*, John Wiley & Sons, Ltd, Chichester, UK, 2009, pp. 227–453.
35 Y. Lu, F. Hasegawa, Y. Kawazu, K. Totani, T. Yamashita and W. Toshiyuki, *Sen'i Gakkaishi*, 2004, **60**, 165–172.
36 O. Nuyken, T. Kneppe and B. Voit, *Macromol. Chem. Phys.*, 1989, **190**, 1015–1024.
37 A. Ajami, W. Husinsky, M. Tromayer, P. Gruber, R. Liska and A. Ovsianikov, *Appl. Phys. Lett.*, 2017, **111**, 71901.
38 R. Dědic, A. Svoboda, J. Pšenčík and J. Hála, *J. Mol. Struct.*, 2003, **651–653**, 301–304.
39 M. Lunzer, L. Shi, P. Gruber, M. Markovic, D. Ossipov, R. Liska and A. Ovsianikov, *Angew. Chemie*, submitted.
40 N. Kamigata and M. Kobayashi, *Sulfur Rep.*, 1982, **2**, 87–128.
41 Farbenfabriken Bayer Aktiengesellschaft, *US* 2911336A, 1959.
42 E. I. du Pont de Nemours and Co, *DE* 2405855, 1974.
43 P. Müller, H. Müller-Dolezal, H. G. Padeken, R. Stoltz and H. Söll, in *Houben-Weyl Methods of Organic Chemistry Vol. X/3, 4th Edition: Diazonium Salts; Azo-, Azoxy-Compounds II; Diazenes II; Azides; Nitrile Oxides*, Thieme, 2014, pp. 570–585.
44 J. G. Parker, *IEEE Circuits Devices Mag.*, 1987, **3**, 10–21.
45 F. Wilkinson, W. P. Helman and A. B. Ross, *J. Phys. Chem. Ref. Data*, 1995, **24**, 663–677.
46 E. Skovsen, J. W. Snyder, J. D. C. Lambert and P. R. Ogilby, *J. Phys. Chem. B*, 2005, **109**, 8570–8573.
47 R. W. Redmond and J. N. Gamlin, *Photochem. Photobiol.*, 1999, **70**, 391–475.
48 M. Korinek, R. Dědic, A. Svoboda and J. Hála, *J. Fluoresc.*, 2004, **14**, 71–74.
49 M. Boncler, M. Różalski, U. Krajewska, A. Podsędek and C. Watala, *J. Pharmacol. Toxicol. Methods*, 2014, **69**, 9–16.
50 C. F. Cesarone, C. Bolognesi and L. Santi, *Anal. Biochem.*, 1979, **100**, 188–197.